An ensemble WideResNet learning-based approach for classification of multi-class colorectal cancer tissue types in histology images

Mahdi Masrori[1], Masoomeh Dadpay[1*], Khosro Rezaee[2**], Hamed Naghoosi[3], Hamed Bagheri[1], Sandra Saeedi[1]

[1] Cancer Epidemiology Research Center, Aja University of Medical Sciences, Tehran, Iran.
[2] Department of Biomedical Engineering, Meybod University, Meybod, Iran.

[3] Infectious Diseases Research Center, Aja University of Medical Sciences, Tehran, Iran

Corresponding Authors
First: Masoomeh Dadpay, e-mail: mdadpay1@gmail.com, ORCID ID: https://orcid.org/0000-0001-6384-4794.
Second: Khosro Rezaee, e-mail: kh.rezaee@meybod.ac.ir. Tel: +98-35-32357500, Fax: +98-35-32353004. ORCID ID: https://orcid.org/0000-0001-6763-6626

Abstract

Histopathology imaging (HI) plays a significant role in enhancing the prognosis of colorectal cancer (CRC), which ranks as the second leading cause of cancer-related deaths globally. Classifying colon cancer tissues with HI can be challenging due to differences in morphology, the presence of artifacts when recording microscopic images, and the lack of histological expertise. The use of WideResNet network structure as a novel method for identifying textures in HIs is proposed using deep feature maps extracted from direct HIs and correlation matrices inputs. By using HSV (Hue, Saturation and Value) space, the first step is to decrease various artifacts during HI recording. After designing the ensemble model, the suggested structure has been evaluated and validated using the datasets CRC-5000 and NCT-CRC-HE-100K. On the CRC data set, the ensemble model had accuracy of 98.71% and 99.13%. Deep ensemble learning performed better than current methods in terms of computational and temporal performance, according to the results. Our proposed method is generalizable and has been tested on many of unseen HIs. Based on their data, pathologists can classify unseen Whole Slide Images (WSIs) images using only their lesion classes. The proposed tissue analysis mechanism reliably predicts CRC when pathological images are accurate.

Keywords: Colorectal cancer, Histopathology image, Deep transfer learning, Computational pathology, Ensemble learning, Correlation matrices.

1- Introduction

The third most common cancer type in the world is colorectal cancer (CRC), which is responsible for about 10% of cancer-related deaths worldwide [1]. The Centers for Disease Control and Prevention (CDC) reported 1.1 million newly reported cases and 551,000 deaths in 2018 [2]. The World Health Organization (WHO) predicts that 75 million cases will develop colon cancer by 2030, 17 million of whom will die and another 27 million will develop the disease. Clinical outcomes, however, can differ significantly between patients with resectable diseases. Tumor symptoms encompass several factors such as type 2 diabetes, nutritional deficiencies, diabetes, obesity, and smoking, which have been found to be associated with reduced odds of survival [3, 4]. CRC typically recurs in 60 to 80% of cases and 95% within four years of resection [4,5]. Colon malignancies are frequently identified by the utilization of needle biopsy or fine needle aspiration (FNA) techniques [5,6]. When cells or tissues are mounted on whole slide images, they can be observed under a microscope. Over the years, the histopathological imaging (HI) approach to the CRC has been well established. HI analysis has been shown to be highly effective in colorectal cancer clinical evaluation [7, 8]. In order to confirm colorectal cancer research and treatment, it is necessary to identify tumor sites, measure disease progression, and classify cancer prototypes from complete patient slide images [9, 10]. Visualizing, staging, and grading rectal cancer is possible.

During lengthy HI analyses, the pathologist's knowledge, skills, and abilities are vital. In addition, unfavorable traits including weariness and concentration issues are linked to the HI analytical procedure. Colorectal cancer (CRC) diagnosis has been improved through automated techniques. In order to improve the outcomes of their decisions, efforts have been made [10]. Computer-aided design (CAD) solutions can be developed that reduce pathologists' workload by combining image processing techniques with machine learning techniques. Furthermore, it reduces the time needed to read and evaluate health-related data, speeds decision-making. If diagnosed early, CRC treatment is more likely succeed. Automated detection technologies can make it easier to detect CRC at an early stage. The most difficult obstacle to overcome is developing techniques for separating HI medicinal properties extracted from intestinal tissues. Although handcrafted extracted features take longer to define tissue status, when combined with other techniques, they are unreliable for producing distinctive characteristic vectors for classification.

As well as providing use cases for CAD models, deep learning (DL) models have also been shown to be effective for medical purposes [11,12]. DL networks face various challenges such as the need for large amounts of data to perform, the high educational costs associated with complex information patterns, and the lack of generally accepted assumptions to select the proper DL architecture [13,14]. Some machine

learning technology uses a created pattern to solve problems that need automation, and in this way, technological knowledge transfer occurs [15,16]. In the meantime, DL and in a better sense, deep transfer learning (DTL) architecture is aimed at transferring learning in DL based systems to another task in classification [17].

Previous studies used handcrafted features to compensate for low classification rates due to high processing costs and low HI quality. In the study [18], the authors demonstrate the different characteristics of malignant tumors. Thus, their methods incorporate unsupervised feature embedding and clustering [19]. Traditionally, CRC tumors are classified by liver pathology imaging based on DTL analysis. In CRC research, DL techniques based on HI analysis are crucial.

The primary responsibility of a pathologist is to determine the stage of a malignant tumor. Several subtypes of cancer can be distinguished from each other. Choosing the type of tissue to be treated is the first step in creating a treatment strategy. Overfitting is the key concern here, since it impacts accuracy and precision. Since the images have a high degree of textural similarity, it is imperative to employ an automated method to maximize the learning process. It is possible reduce absolute errors by utilizing DL techniques. In order to provide accurate classification and automate CRCs, deep learning requires many images. As a result of this study, the DTL model used to classify CRCs has been improved. To reliably classify HI, Residual Networks (ResNet) needs a small number of training pictures and a large number of colon tissue classifications.

The complexity of analyzing HIs is exacerbated by the absence of annotated histopathology pictures and the presence of several color spaces. Since histopathology focuses on tissues rather than specific structures, capturing histopathological images presents a challenge. Based on the WideResNet architecture, ensemble feature generation and learning methods are used to develop our proposed system, and the results are estimated. The purpose of this study was to fill the gaps in previous research, in particular low classification accuracy and multi-class analysis of histopathological images. This study can contribute to a number of areas.

- Specifically, the ultimate goal of this study is to develop novel and distinctive DL structures. In order to improve the classification of features, we started by adding information about color space, saturation, and value. Primarily, our objective is to discover an improved method for classifying features according to their HSV properties. Using HSV instead of RGB color space, pictures of histopathological lesions of color combine with homogeneous light and reduce the influence of artificial colors. A second stage utilizes transfer learning (TL) to increase performance by accessing a variety of feature maps.
- It is our understanding that no deep learning method has been proposed to date that uses cumulative feature extraction and multi-class classification of HIs to find CRC. As a second input to the

proposed structure, each HI image is also associated with the correlation procedure to generate the two-dimensional correlation matrix.

- It is possible to distinguish between several different types of CRC using HI analysis. By adopting this new strategy, the possibility of uncertainty and generalizability has been significantly reduced. The technique is unaffected by the presence or absence of high-contrast or high-quality information in the image.
- Various methods of algorithm training and testing have been considered in order to achieve the desired results. For cross-validation (CV), 100,000 HIs from two separate histopathology pictures were employed.

Accordingly, our research is organized as follows. Section 2 provides a brief overview of the related research. Section 3 discusses the novel technique for ensemble feature extraction and learning that is based on an optimized DTL structure described in Section 3. The experimental outcomes achieved with the suggested HI analysis approach are summarized in Section 4. A summary of the major points discussed in Section 5 follows the conclusion of this study.

2- Related work

As opposed than conventional approaches that extract their characteristics from the texture of high-resolution images, DL methods produce a uniquely descriptive description directly from the raw image.

Srinukunwattana et al. [7] developed a technique for identifying and classifying nuclei in a variety of settings using in-depth learning (miscellaneous, inflammatory, epithelial, and fibroblastic).

The contour segmentation technique and convolutional neural network (CNN) architecture were used by Haj Hassan et al. [20] to differentiate CRC tissues from multispectral HI. The three types of tissue associated with CRC degrees could be consistently identified using segmented HI areas, namely carcinoma (CA), intraepithelial neoplasia (IN), and benign hyperplasia (BH).

Izoka et al. [21] used whole-slide images (WSIs) of gastric and colorectal tumors to diagnose tumors by training recurrent neural networks (RNNs) and CNN architectures. Researchers correctly identified three types of WSI images in three different types of tissue: adenomas, adenocarcinomas, and non-neoplastic tissues.

A reliable computer-aided design (CAD) strategy was developed by Kwak et al. [22] to identify lymph node metastasis in patients with colorectal cancer using a combination of high-resolution imaging (HI) and feature interpretation. Based on the CNN framework, they developed a deep learning model for detecting CRC texture, which was then applied to a variety of real-world situations.

Additionally, Korbar et al. [23] devised a CAD method for identifying colonic polyps that could be used to visualize them.

Using high-resolution colon images, Manivan et al. [24] analyzed the endocrine systems. Their algorithm combined the features of a hand-made multiscale image with those calculated by a deep learning algorithm designed to convert segmentation predictions into results. A comparison was made between the developed system and the GlaS dataset.

Hu et al. [25] combined the deep learning ResNet-101 model with the recurrent CNN to eliminate glandular segmentation from their results. Their blood test was able to distinguish high-risk characteristics of cancer and dysplasia with an AUC of 0.91 and a sensitivity of 97.4%.

Using CNN and multi-channel attention mechanism models, Chen et al. [26] classified colorectal histopathology images at the initial stage. The second step training set included incorrect classification images again, improving the model's accuracy. In their dataset, they achieved 98.98% classification accuracy, and in the HE-NCT-CRC-100K dataset, they achieved 99.77% classification accuracy.

A proposed method of patch aggregation based on CNN structure has been proposed by Wang et al. [27] for the diagnosis of colorectal cancer clinics, according to which fragments of poorly labeled patient slide images could be pasted. Prior to their public dissemination, HIs' methodologies were refined and evaluated by a substantial sample of participants. Based on the calculated Kappa value, it averaged 0.896. According to the results of this study, the area under the curve (AUC) for CRC diagnosis exceeded not only the performance of pathologists, as indicated by AUC values of 0.98 and 0.97, but also all other procedures examined.

Riasatian et al. [28] combine histopathological images in various topologies to distinguish between tumor types. The KimiaNet [28] network consists of several dense blocks based on DenseNet. In the Atlas of Cancer Genome Database, there are 7126 slide images of human pathology samples embedded in formalin-fixed paraffin made from 240,000 images collected at 20 magnifications. We evaluated KimiaNet's search and classification capabilities using three publicly available datasets: CRC images, endometrial cancer images, and the Cancer Genome Atlas.

Kassani et al. study [29] presented empirical support for the effectiveness of using transfer learning and CNN modules inside the encoding component of a segmentation framework. A comprehensive and comparative examination was undertaken to address the complex histology segmentation challenge. This study illustrated the advantages of including deep modules into the segmentation encoder-decoder network and elucidated the distinct functionalities of its different components.

Raju et al. [30] proposed a CNN architecture based on deep learning models for HI multiclass categorization. This discovery was made by employing three distinct deep learning models. The most effective model was the recommended adaptive Resnet152 model, producing 98.38% accuracy. Additional models included in the study encompassed VGG16, which achieved an accuracy rate of 96.16%, and a customized iteration of Resnet50, which yielded a higher accuracy rate of 97.08%. A

colorectal imaging multiclass dataset of 5000 images across eight classes. In this study, the researchers utilized image augmentation techniques to generate a dataset consisting of 15,000 images. This was achieved by applying proportionate enhancements to all classes within the dataset.

Bokhors et al. [31] employed artificial intelligence (AI) methodology for segmenting distinct tissue compartments within whole-slide images stained with H and E. This technique was intended to enhance tissue architecture and composition. The present work assessed a range of advanced loss functions applicable to segmentation models. It also offered guidance on their use in HI segmentation. This was achieved through an analysis of a multicentric cohort including CRC patients from five medical institutions located in the Netherlands and Germany. Automated models were employed to develop a CAD approach aimed at classifying colon samples into four distinct categories based on their pathogenic significance.

Khazaee et al. [32] proposed the utilization of a dilated ResNet (dResNet) architecture along with an attention module to generate deep feature maps for tissue classification in HIs. The utilization of Neighborhood Component Analysis (NCA) also mitigates computational complexity. The hybrid technique was verified and evaluated using the NCT-CRC-HE-100 K and CRC-5000 datasets. The hybrid model's accuracy on CRC datasets was 99.5 percent.

Compared to other tissues like breasts and prostates, CNN's development for colon histology is behind. Through the combination of their hybrid model with a modified DTL structure, we may be able to avoid issues such as overfitting, inadequate learning, and uncertainty. Rather than relying on pre-existing datasets or binary classes, researchers developed their own segmentation model and trained and evaluated it on a wide range of educational pictures (tumor or non-tumor). When applied to a WSI colon biopsy, machine learning is able to detect epithelial tumors, even when the background is benign as shown in the case study. In the field of colon histology, DL plays a very important role, as demonstrated in this study.

3- Methodology

An overview of the introduced method illustrated in **Fig. 1** how CRC is detected in HI. The sections of the introduced method are explained below.

3-1 RGB to HSV color

Since staining blends hues, HI images are inherently difficult to evaluate. In order for the HI processing phase to produce natural light homogeneity, the hue, saturation, value (HSV) color space, which includes color, saturation, and brightness, is necessary. HSV color facilitates the understanding of the correlation between image surface and perceived light intensity. Given that d=M-m, m=min (R, G, B), and M=max

(R, G, B), they provide a precise calculation of the H section. The values of r, g, and b may alternatively be determined using *b= (M-B)/d*, *g= (M-G)/d*, and *r= (M-R)/d*.

Since HSV's brightest color is relatively similar to white light, light scattering at high colors intensities can be minimized, which results in a homogeneous signal. Due to this effect, objects appear brighter and redder in bright light. However, dim light makes these objects appear darker. The method of HI is highly sensitive to light leakage, hence requiring the use of a point light source in the RGB color space. The HSV converter employs a processed RGB image to ensure uniform brightness levels. The **Fig. 2** illustrates how to transform a RGB image into an HSV image.

3-2 Deep CNN architecture

CNNs are a sort of neural network that was invented [33]. The primary convolutional equation (1) was solved using a sequence of convolutional filters, and non-linearity was incorporated into this architecture. Numerous machine learning issues have been solved with remarkable results. A CNN's architecture is hierarchical. The following layers x_j (Equation 1) are calculated from the input signal x:

$$x_j = -1 + (\rho W_j x_j) \tag{1}$$

Despite the fact that W_j is a linear operator, there is a non-linearity involved. In addition, W_j is typically used as a convolutional layer in a CNN, and is either a rectifier max(x;0) or a Sig (exp (-x) + 1)$^{-1}$. Let W_j be a stack of convolutional filters. Each layer is a filter map, and its convolutions are defined as the sum of the previous layer's convolutions (Equations 2 and 3).

$$x_j(u, k_j) = \rho\left(\sum_k (W_{j,k_j}(.,k) * x_{j-1}(.,k))(u)\right) \tag{2}$$

$$(g * f)(x) = \sum_{u=-\infty}^{\infty} g(u) f(x-u) \tag{3}$$

Convex optimization problems were used because of their numerous benefits, including their computational tractability and unique optimal solutions. Moreover, stochastic gradient descent is used to train the weights W_j, and the gradients are usually obtained by backpropagation. Data dependence is one of the key challenges associated with deep learning. Contrary to more traditional machine learning techniques, deep learning is primarily taught on massive amounts of data. In order to train the underlying data patterns, vast amounts of data are required. The benefits of HI processing include the development of intelligent technology as well as the diagnosis of many diseases. Consequently, it is necessary to monitor for diseases on a continuous basis and to properly design the decision-making architecture. We need an automated decision-making system capable of a variety of implementation capabilities, such as real-time detection of cancer, lesions, or aberrant tissue in HIs, to communicate with an expert monitoring system in a medical situation.

3-3 Ensemble WideResNet

The Equation 4 delineates a residual block that incorporates an identity mapping.

$$x_{l+1} = \mathbb{N}(x_l, W_l) + x_l \tag{4}$$

The function $\mathbb{N}$ is commonly regarded as a residual function, whereas W_l is used to denote the block parameters. The variables x_{l+1} and x_l are representative of the input and output of the l_{th} unit inside the network. A residual network is comprised of residual blocks that are organized in a preset order. Residual networks employ two essential construction components. The initial component is a convolutional layer, extracting distinctive characteristics from the input. The second unit comprises a fully connected output layer that utilizes the characteristics extracted in the preceding step. In other hand, we have two parts. The simple component comprises of two consecutive convolutions, each with a size of 3 × 3. Moreover, Batch normalization and Rectified Linear Unit (ReLU) activation function are applied between these convolutions. The convolutional operation of a 3 × 3 filter followed by another convolutional operation with **Fig. 3**(a). The second component is a bottleneck including a solitary 3 × 3 convolution encircled by 1 × 1 convolutional layer that concurrently reduce and expand the input dimensionality. The sequence of convolutional operations consists of a 1 × 1 convolution, followed by conv1×1, conv3×3, and conv1×1 as shown in **Fig. 3**(b). The final structure is shown in **Fig. 3**(c), which uses two 3 × 3 convolutional layers and a dropout part.

After analyzing the features, the WideResNet structure will build the set of features used in the next step. The two-dimensional correlation matrix is derived from the pixels of each HI image and is used as the second input to the structure. WideResNet deep extracted features are employed to predict relationships between different variables. This correlation matrix can be used to gain insight into the underlying structure of the data and make predictions about features. By using a deep learning model, such as WideResNet, it is possible to learn complex relationships between different variables in HIs. This model can then be used to predict the value of a given variable based on its correlation with other variables. Thus, the Pearson Correlation Coefficient Matrix (PCCM) was also used to calculate correlation coefficients between signal features [34,35]. In our analysis, each HI was treated as a node (that is, both the original and HSV images). Pearson correlation coefficient was used to determine the correlation between the two histopathology images. PCC uses the Equation 5:

$$\rho_{X,Y} = \frac{cov(X,Y)}{\sigma_X \sigma_Y} \tag{5}$$

X and Y are the feature vectors of two different input HIs. Furthermore, σX represents X's standard deviation, and $Cov(X,Y)$ denotes the covariance (COV) between X and Y. Besides, σY shows the standard deviation (STD) of Y. As a function of the mean and expectation, the $Cov(X, Y)$ is written as Equation 6:

$$Cov(X, Y) = E[(X - \mu_X)(Y - \mu_Y)] \quad (6)$$

Assuming μX is the mean of X and E is the expectation. Therefore, Therefore, it can be concluded from Equation 7 that:

$$\sigma^2 X = \left(E(X - E[X])\right)^2 = E[X^2] - [E[X]]^2 \quad (7)$$

The classification prediction model for CRC based on HI is derived from a modified WideResNet model. The proposed model effectively incorporates ResNet networks, where one network is provided with the HI image and the other network receives the corresponding Pearson correlation coefficient matrix. Initially, the fully connected layers of the two networks were merged, and the output of the convolutional layer was then directed to a unified fully connected layer. The classification process was accomplished by integrating feature maps derived from the signal with feature maps made from the correlation coefficient matrix of histopathology images. The signal properties for each channel were extracted based on various tissue characteristics. In order to enhance the model's accuracy, we calculated a matrix of Pearson correlation coefficients for the aforementioned features. Following the fully connected layer, a SoftMax layer was included to specify the input labels. To optimize the model's training efficacy, we provided a signal and the Pearson correlation coefficient matrix as inputs to two ResNet networks, and then recorded the resultant weights. The proposed ResNet architecture can be seen as an improved version of the commonly employed WideNet design. Ensemble learning, incorporating three distinct modified architectures, where concatenated features are employed in fully connected layers, has the potential to yield significant enhancements. The inclusion of these weights in the provided model can be attributed to the training process using two distinct ResNets. Accordingly, the proposed structure consists of the inputs extracted through the model and a matrix that relates the features together. After passing through the convolutional structure, these inputs are finally concatenated together. Each channel's output characteristics were extracted from HIs, and a Pearson correlation coefficient matrix was then produced and included in the model. After the fully connected layer, a SoftMax layer was used to specify the input label. ResNet networks were trained using the same input HIs (HSV), as well as the corresponding Pearson correlation coefficient matrix, with weights stored to improve the model's training. Due to the fact that the new model was trained using two unique ResNets, these weights are incorporated. **Fig. 4** illustrates the proposed architecture.

Based on the literature [35], WideResNet provides features to classify images, recognize objects, and identify anomalies. These features can be extracted using transfer learning and deep learning. High-level features refer to features that are extracted from the input image and can be used to discriminate between different classes. Deep WideResNet can provide shape, texture, and color. These features can then be utilized to classify HIs, detect objects, and find anomalies in HI images. These features can also be used to detect and diagnose diseases, such as cancer, and to automate medical image analysis. In addition, these features can also be used to improve the performance of medical imaging systems.

4- Experimental results

4-1 Dataset

Data were received from the Medical Center of the University of Mannheim (Germany), which was previously mentioned [36]. **Fig. 5** illustrates that tumors are made up of eight different types of tissues. The cancer epithelium is followed by (1) stromal cells, (2) stromal tissue, (4) inflammatory cells, (5) mucosa and debris, (6) glandular mucosa, (7) adipose tissue, and (8) background. There are 5000 images in the collection with a 150 × 150-pixel resolution and 74 × 74-micrometer resolution.

Staining is usually visible on the images that a pathologist needs to make an accurate diagnosis. The pathologist can distinguish them from one another by using additional histological markers, such as formalin. The images in this dataset have been labeled by experts.

The NCT-CRC-HE-100K histopathology imaging kit is a publicly accessible collection of 100,000 images divided into nine distinct classes each with an aspect ratio of 224 × 224 pixels and an average pixel size of 0.5 millimeters. The nine types of tissues that can be analyzed are as follows: adipose tissue (ADI), normal colon mucosa (NORM), colorectal cancer (CRC), debris (DEB), hematoxylin-eosin (HE), lymphocytes (LYM), mucus (MUC), smooth muscle (MUS), NCT, and cancer-associated stroma (STR).

4-2 Setting

The computational system used in our technique was equipped with a Core i-7 CPU and 16 GB of RAM. A variety of web-based add-ons and toolkits are included in Matlab's software environment. The computer is not equipped with a dedicated electronic graphics processing unit (GPU). In order to construct training, testing, and validation sets, the data can be split into three groups with a ratio of 60-20-20. With a primary learning rate (μ) of 0.002 and 100-1000 iterations, the models have been trained to be effective in the real world.

Moreover, the mini-batch size was limited to 32 and the early-stopping period was limited to 10 epochs in the absence of accuracy gain. We applied the Root Mean Square Propagation (RMSprop) method, as well as momentum and the Stochastic Gradient Descent (SGD) method, to this optimization problem. To prevent the over-fitting challenge within the suggested DL structure, we combined dropout and early-stopping strategies when defining the optimal training iteration. When we fine-tuned the network, we incorporated a Softmax layer as classification layer, which was achieved by replacing the final three layers with a Fully Connect (FC) component. The bias learn rate factor (value of 20) and weight learn rate factor (value of 10) needed to be set to values that were higher than those used in the traditional structure in order to accelerate learning in the new layers. During the tuning phase, a bias learns rate factor of 20 and a weight learn rate factor of 10 were employed.

4-4 Evaluations

For detecting distinct classes (textures found in HI) and classifying CRCs based on HI, we compared family-based ResNet learning algorithms to WideResNet ensemble architecture. The WideResNet Ensemble is employed in both datasets, as seen by the data presented in **Table 1** and **Table 2**, in order to ensure optimal performance in feature extraction. According to the findings shown in **Table 1**, it is evident that many categories may be assigned to each class within the initial dataset, ranging from 1 to 8 categories.

For feature extraction, ResNet DTL algorithms were employed, but the rest of the methodology remained unchanged. Ensemble learning determined the best classifier, for example. WideResNet's ensemble learning approach has proven considerably effective overall as a result of its contribution to the classification process.

The suggested method has also been compared with similar methods such as BasicResNet, ResNeXt, and WideResNet. Despite the fact that the suggested DL feature extraction approach outperformed the others in some aspects, other models within the ResNet architecture families occasionally showed a medium classification error. The results in **Table 1** and **Table 2** indicate that learning can be improved by increasing the classifier associated with the right deep transfer method and its ensemble processes. With the suggested methodology and a small number of replications, it is possible to generate relevant feature maps of histopathological images in just a few minutes. Certain transfer techniques that rely on time transfer might be computationally intensive, especially during the training phase. Consequently, these approaches may not be appropriate for real-time applications. However, it is worth noting that deeper structures can potentially provide improved features in certain situations.

The confusion matrices of the classification process for the first and second HI datasets are depicted in **Figs 6** and **7**. To define the choice technique and maintain the processing time, possible accessible features were used to classify by DTL structures and identify the approach to use. Studies have shown that between 98 and 99 percent of the variation in CRC accuracy measurements is caused by HIs. Based on the extracted features and CRC challenges, a classification method was developed using two datasets. According to the test findings, both datasets were assigned suitable classification forms.

Validation data had an average accuracy of 98.64 percent. Based on the distribution of anticipated classes from the confusion matrix, the accuracy of the test data in both portions of **Fig. 6** was independently determined. The same output is shown in **Fig. 7**, which reaches a 99.16 percent accuracy rate on both test data sets derived from the second HI dataset. A total of 98.98 percent of HIs were accurately classified.

The inclusion of characteristics obtained by automated processes, together with the process of learning the dataset, can lead to a notable improvement in classification accuracy. This is despite the possibility of

the findings being less precise than the original dataset. We demonstrate in scenario 2 that the classification approach has the same level of reliability by using a second data set with a large number of HIs. Using the method described here, CRC tissues of different types can be identified. Additionally, it achieved 99 percent accuracy when dealing with a wide variety of texture classifications, indicating that the extraction of the suggested feature and the developed learning methods obtain a reasonable level of generalization and certainty. The results show that the proposed model is competitive in terms of colorectal cancer classification and diagnosis.

In classification problems with multiple thresholds, the Area Under the Curve of the Receiver Operating Characteristics (AUC-ROC) can be used to measure performance. By analyzing the AUC, we can determine the level of discrimination. Plotting ROCs demonstrates that the model is able to distinguish between various types of CRC in HIs. **Fig. 8** shows the results of a series of studies in which the AUC values for four different classes of unseen HIs were calculated. Because this is a multi-class mode of CRC, the logic for drawing a curve relies on the classification of one class against another. The first two diagrams in Fig. 7 depict unseen data from dataset 1, and the second two diagrams show the classification and plotting of ROCs in dataset 2. In Fig. 8 in part (a), respectively, the AUC values for classes 1 to 8 are equal to 0.984, 0.988, 0.994, 0.987, 0.995, 0.989, 0.997, and 0.993, and for part (b) are corresponding to 0.989, 0.984, 0.985, 0.988, 0.977, 0.988, 0.995, and 0.992. Moreover, in part (c), respectively, the AUC values for classes 1 to 8 are equivalent to 0.984, 0.988, 0.994, 0.987, 0.995, 0.989, 0.997, and 0.993. For part (d) are equivalent to 0.989, 0.984, 0.985, 0.988, 0.977, 0.988, 0.995, and 0.992. Moreover, in part (c), respectively, the AUC values for classes 1 to 8 are equal to 0.993, 0.993, 0.995, 0.995, 0.994, 0.995, 0.997, 0.997, and 1.000. For part (d) are equal to 0.993, 0.991, 0.996, 0.995, 0.993, 0.994, 0.996, 0.997, and 1.000.

4-4 Discussion

The proposed approach must be capable of classifying tumors and colon tissue into at least two distinct groups in order to identify them and categorize them. As a result, clinicians can more accurately diagnose patients. Each approach is used for a different purpose in the classification of CRCs. It is vital that a record of similar cases be available to make an accurate diagnosis. A pathologist uses microscopic criteria to diagnose sick slides, including the color, size, texture, shape, and blackness of cells. According to early research [37], color information can be preserved by retaining the HSV color space. HIs can be employed to detect healthy cells from malignant cells based on their hues. If the color of a histopathological image is to remain constant, then the original color must be preserved. The HSV color representation is more realistic than RGB because it more closely resembles how humans perceive color. However, lighting and

contrast may make it difficult to distinguish the correct features. Therefore, an HSV color model was proposed, which preserves color while addressing challenges outside the model's scope.

By incorporating a wideResNet structure into an ensemble, meaningful features can be extracted at a suitable level of processing complexity. As a result of WideResNet's structure, it is simple to develop a architecture with many layers, thereby reducing the number of training and testing errors. In contrast to earlier learning architectures, WideResNets uses identity mapping to avoid disappearing gradients. WideResNet's residual blocks eliminate the problem of vanishing gradients. Ensemble learning in networks is enabled by convolutional layers, which are the last bottleneck blocks. An ensemble is more effective than a single model because it can make more accurate predictions and perform better than any single model.

There is a significant difference between the rate at which deep learning algorithms converge and the credibility of their results. The WideResNet technique outperformed the other two in terms of relevant attributes and convergence speed (e.g., in comparison with BasicResNet and ResNeXt architectures). In order to obtain the most accurate results for feature extraction, it became increasingly critical that CRC classification be reliable and robust in order to handle the growing number of His classes. As seen in **Fig. 9 (a)**, the first set of HIs investigated during the deep learning model's initial phase produced the best results in terms of accuracy and loss computations. Using loss and accuracy computations, we can build a deep learning model based on the last two components of **Fig. 9 (b)** to reliably identify the sections.

This approach also has a manageable level of computational complexity. In addition, the WideReNet ensemble is useful because it produces related features that are then optimized through the collection mechanism, as shown in **Fig. 10**. In this figure, the values of accuracy, sensitivity, and specificity for an unseen data sample are displayed, which are shown in sections (a) and (b) for datasets 1 and 2, respectively. With our concept, unlike Softmax and End-to-End (e2e) designs, computing complexity is reduced while maintaining high accuracy and competent processing performance. Additionally, an examination was conducted on the computational complexity issue, as well as an evaluation of the effectiveness of the suggested method for feature extraction and ultimate classification.

Table 3 compares the results of similar approaches to the results of the proposed method. In this table, quantitative approaches and the proposed algorithm are compared using NCT-CRC-HE-100K and Kather texture 2016 pictures, demonstrating that the proposed algorithm has a strong multi-class capability. However, the algorithm's results have not yet been tested on unseen data in an analogous fashion. Thus, the generalizability of the suggested technique can be demonstrated with respect to a substantial portion of the HI visual data.

Using the NCT-CRC-HE-100K dataset, Ghosh et al. [38] demonstrated 96.16% accuracy with high computing complexity using ensemble learning based on CNNs to identify various lesions in HIs. We

have improved the accuracy by 2-2.5% compared to this model. In a study by Hamida et al. [39] with 96.6% accuracy, these results were implemented in Kather texture 2016. The NCT-CRC-HE-100K database was also expressed with 99.76% accuracy and low generalization.

The proposed approaches are 0.02 percent less accurate than MCAM and 0.06 percent more accurate than IL-MCAM, according to Chen et al. [26]. Compared to their models, our method has a significant reduction in computing complexity. They also overlooked the intricate nature of the tissue depicted in the photograph, as well as the asymmetrical dispersion of light caused by the staining process, which results in variations in color intensity.

Kather et al. [40] also used NCT-CRC-HE-100K and VGG-16 with TL structures, which reached 98.70%, a little lower than our proposed model. There are a number of challenges in similar approaches, including overfitting, a lack of available HIs, and added artifacts from the environment during the recording of WSIs.

Because early identification of colon cancer is so vital, swift and precise classification of HIs is a crucial stage in the process. To ease pathologists' labor, accurate categorization techniques must perform well in the absence of annotated databases. This research lays out a generalizable technique for overcoming learning and time restrictions, as well as making HI pictures more accessible in clinics and ensuring accurate classifications.

5- Conclusion

Using three WideResNet-based DTL algorithms and effective learning, we classified colorectal cancer (CRC) from histopathology images. An ensemble model of WideResNet modules is proposed to analyze the texture of colorectal cancer histology. When microscopy was used to record various colon tissues, the HSV-based color transform method was used to reduce image artifacts. These features and ensembles were then used to generate a texture with many classes. In both training and testing, the proposed method outperforms conventional deep learning models. Hence, the new model is an effective tool for detecting and classifying colon cancer. Since this method is generalizable and is invulnerable to uncertainty, it is superior to previous similar methods since it retains accuracy even when HIS contains complex components and textures. The generalizability of the Kather texture 2016 and the NCT CRC-HE-100K dataset has been extensively tested. In order to compare histology photographs, we used a variety of unseen HIs. Deep learning models will integrate and reorganize attention processes in the future. Consequently, our research aims to investigate the impact of incorporating attention mechanisms into various components of deep learning architectures on the classification accuracy of convolutional layers.

Funding: No funding was received.

Conflicts of interest/Competing interests: There is no conflict of interest.

References

1- Zhou, C., Jin, Y., Chen, Y., et al., "Histopathology classification and localization of colorectal cancer using global labels by weakly supervised deep learning", Comput. Med. Imaging Graph., 88, p.101861, (2021).
2- Tripathy, A., Dash, J., Kancharla, S., et al., "Probiotics: a promising candidate for management of colorectal cancer", Cancers, 13(13), p. 3178, (2021).
3- van den Berg, I., Coebergh van den Braak, R. R., van Vugt, J. L., et al., "Actual survival after resection of primary colorectal cancer: results from a prospective multicenter study", World J. Surg. Oncol., 19(1), pp. 1-10, (2021).
4- Ottaiano, A., Santorsola, M., Circelli, L., et al., "Hypertension, type 2 diabetes, obesity, and p53 mutations negatively correlate with metastatic colorectal cancer patients' survival", Front. Med., 10, p.1091634, (2023).
5- Jelski, W., Mroczko, B., "Biochemical markers of colorectal cancer–present and future", Cancer Manag. Res., 22, pp. 4789-97, (2020).
6- Metze, K., Adam, R., Florindo, J. B., "The fractal dimension of chromatin-a potential molecular marker for carcinogenesis, tumor progression and prognosis", Expert Rev. Mol. Diagn., 19(4), 299-312, (2019).
7- Sirinukunwattana, K., Raza, S. E., Tsang, Y. W., et al., "Locality sensitive deep learning for detection and classification of nuclei in routine colon cancer histology images", IEEE transactions on medical imaging, 35(5), pp.1196-1206, (2016).
8- Jia, Z., Huang, X., Eric, I., et al., "Constrained deep weak supervision for histopathology image segmentation", IEEE transactions on medical imaging, 36(11), pp.2376-2388, (2017).
9- Sung, H., Ferlay, J., Siegel, R. L., et al., "Global cancer statistics 2020: GLOBOCAN estimates of incidence and mortality worldwide for 36 cancers in 185 countries", CA: a cancer journal for clinicians, 71(3), pp.209-249, (2021).
10- Gadermayr, M., Dombrowski, A. K., Klinkhammer, B. M., et al., "CNN cascades for segmenting sparse objects in gigapixel whole slide images", Computerized Medical Imaging and Graphics, 71, pp.40-48, (2019).
11- Hatipoglu, N., Bilgin, G., "Cell segmentation in histopathological images with deep learning algorithms by utilizing spatial relationships", Medical & biological engineering & computing, 55(10), pp.1829-1848, (2017).
12- Kaushal, C., Bhat, S., Koundal, D., Singla, A., "Recent trends in computer assisted diagnosis (CAD) system for breast cancer diagnosis using histopathological images", Irbm, 40(4), pp.211-227, (2019).
13- Talo, M., "Automated classification of histopathology images using transfer learning", Artificial intelligence in medicine, 101, p.101743, (2019).
14- Mazo, C., Bernal, J., Trujillo, M., et al., "Transfer learning for classification of cardiovascular tissues in histological images", Computer methods and programs in biomedicine, 165, pp.69-76, (2018).
15- George, K., Faziludeen, S., Sankaran, P., "Breast cancer detection from biopsy images using nucleus guided transfer learning and belief based fusion", Computers in Biology and Medicine, 124, p.103954, (2020).
16- Celik, Y., Talo, M., Yildirim, O., et al., "Automated invasive ductal carcinoma detection based using deep transfer learning with whole-slide images", Pattern Recognition Letters, 133, pp.232-239, (2020).
17- Rezaee, K., Badiei, A. and Meshgini, S., "A hybrid deep transfer learning-based approach for COVID-19 classification in chest X-ray images", In 2020 27th National and 5th International Iranian Conference on Biomedical Engineering (ICBME), pp. 234-241, (2020).
18- Kleczek, P., Jaworek-Korjakowska, J. Gorgon, M., "A novel method for tissue segmentation in high-resolution H&E-stained histopathological whole-slide images", Computerized Medical Imaging and Graphics, 79, p.101686, (2020).
19- Amores, J., "Multiple instance classification: Review, taxonomy and comparative study", Artificial intelligence, 201, pp.81-105, (2013).

20- Haj-Hassan, H., Chaddad, A., Harkouss, et al., "Classifications of multispectral colorectal cancer tissues using convolution neural network", Journal of pathology informatics, 8, (2017).
21- Iizuka, O., Kanavati, F., Kato, K., et al., "Deep learning models for histopathological classification of gastric and colonic epithelial tumours", Scientific reports, 10(1), pp.1-11, (2020).
22- Kwak, M.S., Lee, H.H., Yang, J.M., et al., "Deep convolutional neural network-based lymph node metastasis prediction for colon cancer using histopathological images", Frontiers in Oncology, 10, p.3053, (2020).
23- Korbar, B., Olofson, A.M., Miraflor, A.P., et al., "Deep learning for classification of colorectal polyps on whole-slide images", Journal of pathology informatics, 8, (2017).
24- Manivannan, S., Li, W., Zhang, J., et al., "Structure prediction for gland segmentation with hand-crafted and deep convolutional features", IEEE transactions on medical imaging, 37(1), pp.210-221, (2017).
25- Ho, C., Zhao, Z., Chen, X.F, et al., "A promising deep learning-assistive algorithm for histopathological screening of colorectal cancer", Scientific Reports, 12(1), pp.1-9, (2022).
26- Chen, H., Li, C., Li, X, et al., "IL-MCAM: An interactive learning and multi-channel attention mechanism-based weakly supervised colorectal histopathology image classification approach", Computers in Biology and Medicine, 143, p.105265, (2022).
27- Wang, K.S., Yu, G., Xu, C., et al., "Accurate diagnosis of colorectal cancer based on histopathology images using artificial intelligence", BMC medicine, 19(1), pp.1-12, (2021).
28- Riasatian, A., Babaie, M., Maleki, D., et al., "Fine-tuning and training of densenet for histopathology image representation using tcga diagnostic slides", Medical Image Analysis, 70, p.102032, (2021).
29- Kassani, S. H., Kassani, P. H., Wesolowski, M. J, et al., "Deep transfer learning based model for colorectal cancer histopathology segmentation: A comparative study of deep pre-trained models", Int. J. Med. Inform., 159, pp. 104669, (2022).
30- Raju M. S., Rao B. S., "Colorectal multi-class image classification using deep learning models", Bull. Electr. Eng. Inform., 11(1), pp. 195-200, (2022).
31- Bokhorst, J. M., Nagtegaal, I. D., Fraggetta, F., et al., "Deep learning for multi-class semantic segmentation enables colorectal cancer detection and classification in digital pathology images", Sci. Rep.,13(1), pp. 8398, (2023).
32- Khazaee Fadafen M., Rezaee K., "Ensemble-based multi-tissue classification approach of colorectal cancer histology images using a novel hybrid deep learning framework", Sci. Rep., 13(1), pp. 8823 (2023).
33- Ha, I., Kim, H., Park, S., & Kim, H., "Image retrieval using BIM and features from pretrained VGG network for indoor localization", Building and Environment, 140, pp.23-31, (2018).
34- Li, Z., Liu, F., Yang, W., et al., "A survey of convolutional neural networks: Analysis applications and prospects", CoRR, vol. abs/2004.02806, (2020).
35- Zagoruyko S., Komodakis N., "Wide residual networks", arXiv preprint arXiv:1605, 07146, (2015).
36- Kather, J. N., Weis, C. A., Bianconi, F., et al., "Multi-class texture analysis in colorectal cancer histology", Scientific reports, 6(1), 1-11, (2016).
37- Dhal, K. G., Ray, S., Das, S., et al., "Hue-preserving and gamut problem-free histopathology image enhancement", Iranian Journal of Science and Technology, Transactions of Electrical Engineering, 43(3), pp.645-672, (2019).
38- Ghosh, S., Bandyopadhyay, A., Sahay, S., et al., "Colorectal histology tumor detection using ensemble deep neural network", Engineering Applications of Artificial Intelligence, 100, p.104202, (2021).
39- Hamida, A. B., Devanne, M., Weber, J., et al., "Deep learning for colon cancer histopathological images analysis". Computers in Biology and Medicine, 136, p.104730, (2021).
40- Kather, J. N., Krisam, J., Charoentong, P., et al., "Predicting survival from colorectal cancer histology slides using deep learning: A retrospective multicenter study", PLoS medicine, 16(1), e1002730, (2021).

Figures and tables captions

Fig. 1. It is shown in two sections, training and testing, how the approach works.

Fig. 2. The presented figure is a simplified diagram illustrating the sequential steps involved (a) in the conversion procedure of an RGB picture to HSV color space and (b) represents the RGB component in the RGB to HSV color space conversion.

Fig. 3. Various residual networks yield an appealing WideResNet topology. Additionally, it is worth noting that prior to each convolution operation, batch normalization and ReLU activation are applied. However, these steps are omitted from the provided illustration for clarity. In this figure, (a) is basic, (b) is bottleneck, and (c) is WideResNet architecture.

Fig. 4. The framework of the proposed architecture based on ensemble WideResNet.

Fig. 5. A row containing examples from just one class illustrates a sample image from a dataset. HIs from left to right are: (1) background, (2) adipose tissue, (3) mucosal glands, (4) mucosal remnants, (5) immune cells, (6) complex stroma, (7) simple stroma, and (8) tumor epithelium [36].

Table 1. For the first dataset with eight classes, this table presents the accuracy of CRC categorization through HI analysis.

Table 2. For the second dataset with nine classes, this table presents the accuracy of CRC categorization through HI analysis.

Fig. 6. For two different test data, the confusion matrices of the classification process of the first HI dataset are shown in this figure.

Fig. 7. For two different test data, the confusion matrices of the classification process of the second HI dataset are shown in this figure.

Fig. 8. as demonstrated by this figure, the AUC values for four different classes of unseen HIs were calculated. The diagrams a and b show the ROC results for unseen images from dataset 1, and c and d show the ROC results for unseen images from dataset 2.

Fig. 9. For both datasets, we selected several unseen HIs and compared our model with BasicResNet and ResNeXt based on accuracy in (a) and (c) and loss in (b) and (d), respectively.

Fig. 10. As shown in section (a) and (b) for datasets 1 and 2, the accuracy, sensitivity, and specificity values are shown for an unseen sample of data.

Table 3. We evaluate our suggested model against other quantitative approaches using the same data sets.

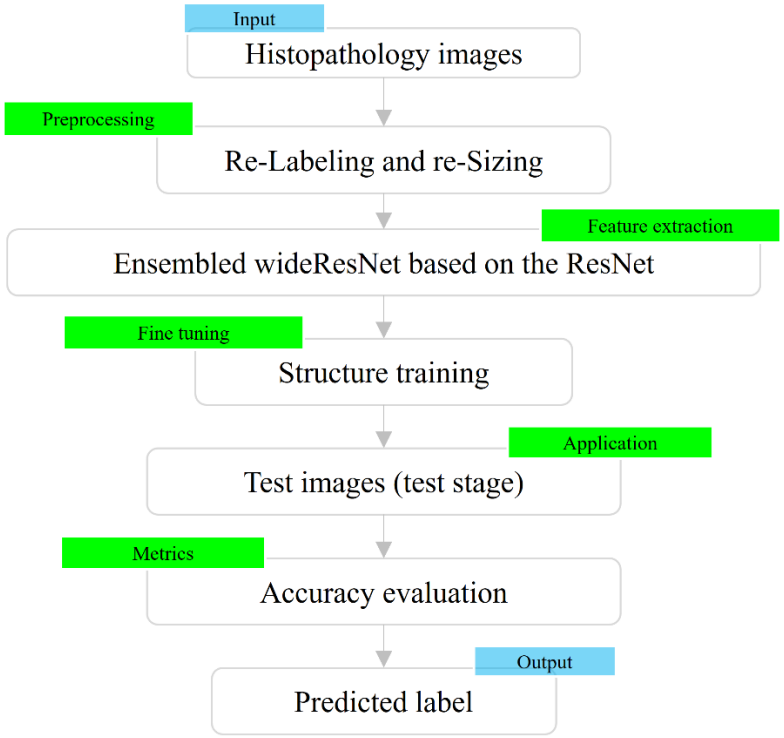

Fig. 1. It is shown in two sections, training and testing, how the approach works

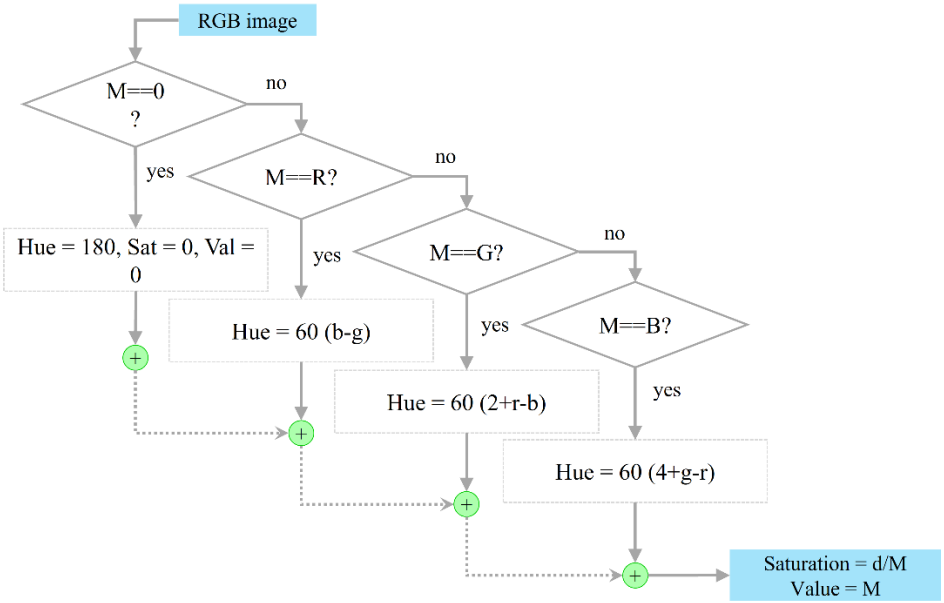

Fig. 2. The presented figure is a simplified diagram illustrating the sequential steps involved (a) in the conversion procedure of an RGB picture to HSV color space and (b) represents the RGB component in the RGB to HSV color space conversion.

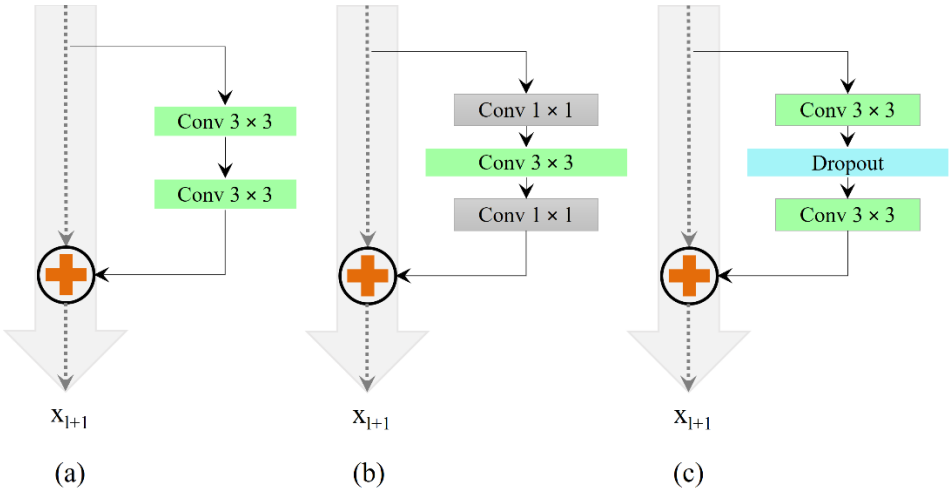

Fig. 3. Various residual networks yield an appealing WideResNet topology. Additionally, it is worth noting that prior to each convolution operation, batch normalization and ReLU activation are applied. However, these steps are omitted from the provided illustration for clarity. In this figure, (a) is basic, (b) is bottleneck, and (c) is WideResNet architecture.

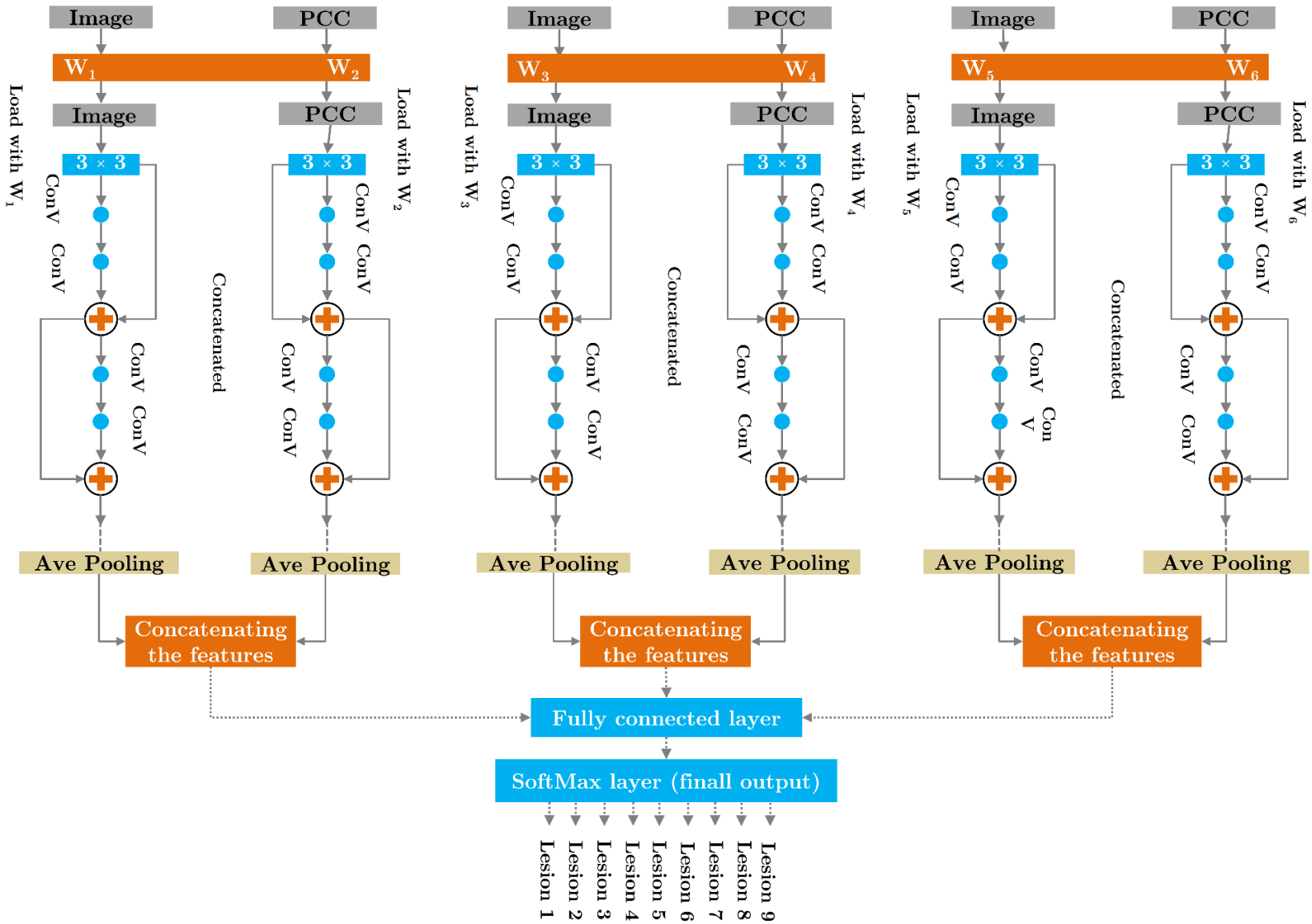

Fig. 4. The framework of the proposed architecture based on ensemble WideResNet.

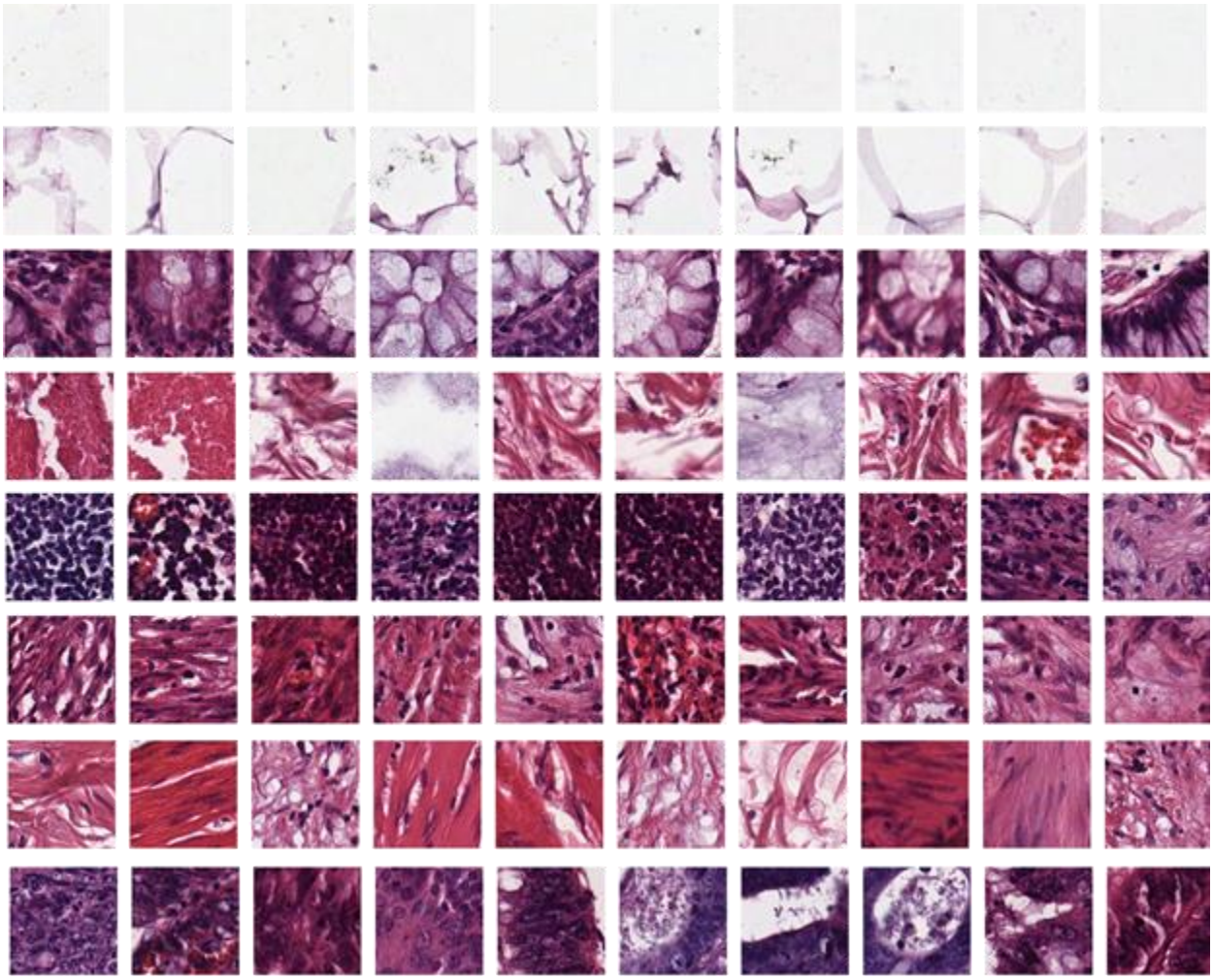

Fig. 5. A row containing examples from just one class illustrates a sample image from a dataset. HIs from left to right are: (1) background, (2) adipose tissue, (3) mucosal glands, (4) mucosal remnants, (5) immune cells, (6) complex stroma, (7) simple stroma, and (8) tumor epithelium [36].

Table 1. For the first dataset with eight classes, this table presents the accuracy of CRC categorization through HI analysis.

Dataset 1	**BasicResNet**		**ResNeXt**		**WideResNet**		**Ensemble WideResNet**	
	Min	Max	Min	Max	Min	Max	Min	Max
Background	97.48	98.19	98.78	98.88	98.78	99.22	99.08	99.62
Adipose	96.54	97.61	97.62	98.17	97.94	98.51	98.19	98.70
Glands	96.59	97.73	97.28	98.11	97.90	98.41	98.39	98.85
Debris and mucus	96.98	97.77	97.64	98.12	98.33	98.93	98.74	99.29
Immune cell conglomerates	96.56	97.83	97.31	98.42	98.07	98.78	98.41	99.12
Stroma (complex)	97.21	97.92	97.49	98.13	98.02	98.65	98.34	98.73
Stroma (simple)	96.54	97.65	97.43	98.10	97.82	98.41	98.03	98.63
Tumor epithelium	96.27	96.91	96.88	97.28	97.10	98.03	97.23	98.44
Average	96.77	97.70	97.42	98.11	97.99	98.61	98.55	98.93

Table 2. For the second dataset with nine classes, this table presents the accuracy of CRC categorization through HI analysis.

Dataset 2	BasicResNet		ResNeXt		WideResNet		Ensemble WideResNet	
	Min	Max	Min	Max	Min	Max	Min	Max
Adipose tissue (ADI)	95.54	97.95	96.08	98.22	98.12	99.73	98.31	99.73
Background (BACK)	96.48	97.22	96.35	98.31	98.27	99.44	98.48	99.44
Debris (DEB)	97.72	98.79	96.67	98.33	98.51	99.28	98.73	99.28
Lymphocytes (LYM)	95.70	96.57	95.42	96.63	97.70	98.38	98.44	99.38
Mucus (MUC)	95.76	97.91	96.36	97.24	98.33	99.41	98.65	99.41
Smooth muscle (MUS)	95.49	97.28	96.09	98.17	97.51	98.28	98.51	99.28
Normal colon mucosa (NORM)	96.54	97.42	96.05	97.49	97.47	98.12	98.47	99.12
Cancer-associated stroma (STR)	95.85	97.19	95.80	97.42	99.67	99.48	99.67	99.48
Adenocarcinoma epithelium (TUM)	96.27	97.03	96.43	98.41	98.82	99.39	98.82	99.39
Average	96.15	97.54	96.13	97.80	98.26	99.05	98.68	99.40

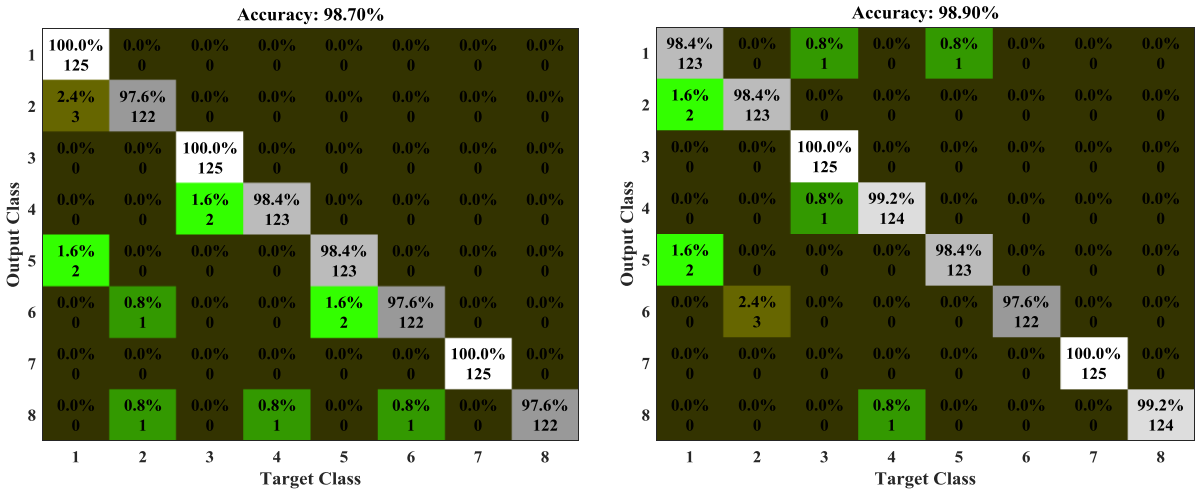

Fig. 6. For two different test data, the confusion matrices of the classification process of the first HI dataset are shown in this figure.

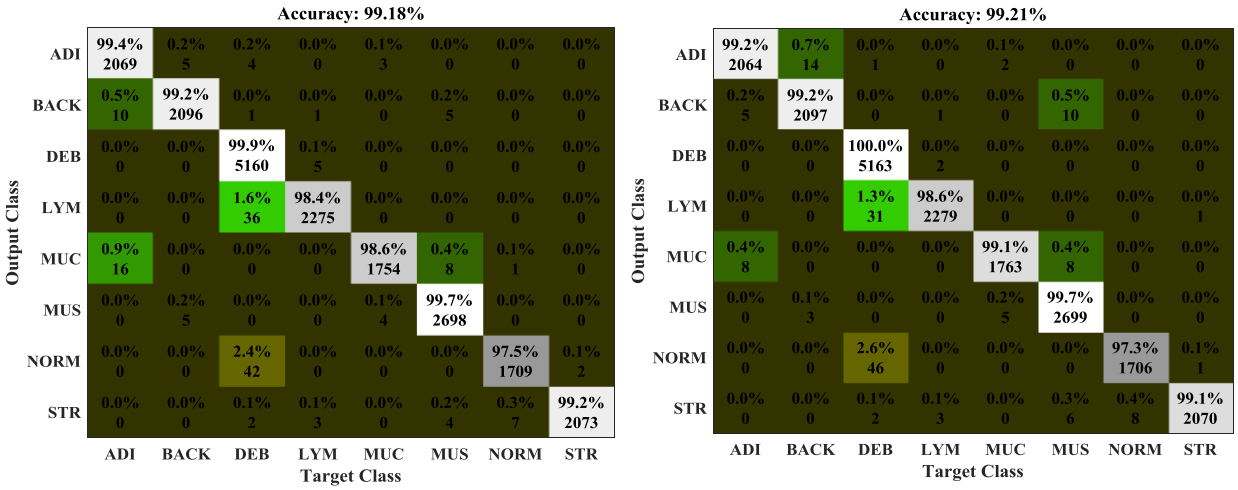

Fig. 7. For two different test data, the confusion matrices of the classification process of the second HI dataset are shown in this figure.

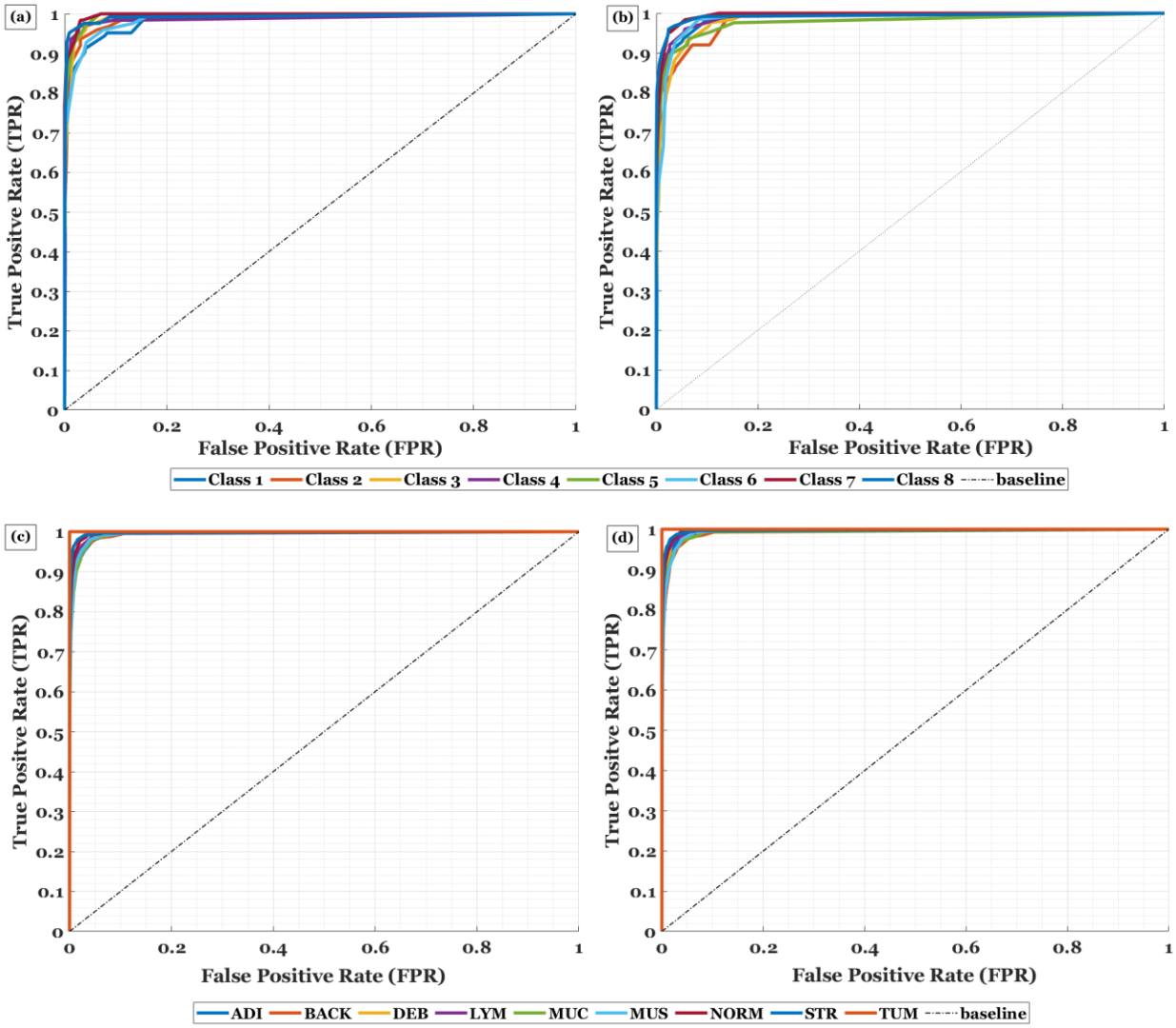

Fig. 8. as demonstrated by this figure, the AUC values for different classes of unseen HIs were calculated. The diagrams a and b show the ROC results for unseen images from dataset 1, and c and d show the ROC results for unseen images from dataset 2.

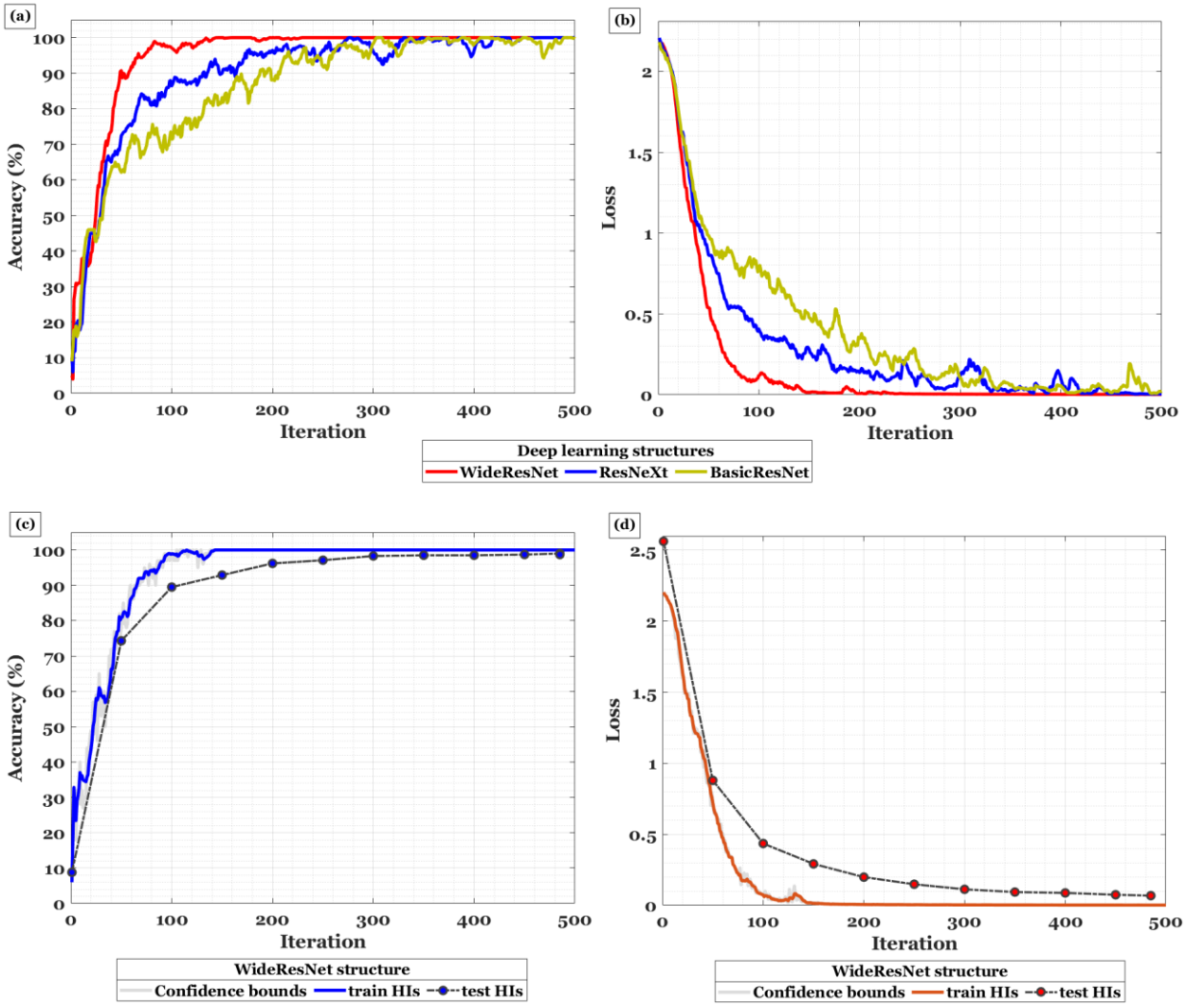

Fig. 9. For both datasets, we selected several unseens HIs and compared our model with BasicResNet and ResNeXt based on accuracy in (a) and (c) and loss in (b) and (d), respectively.

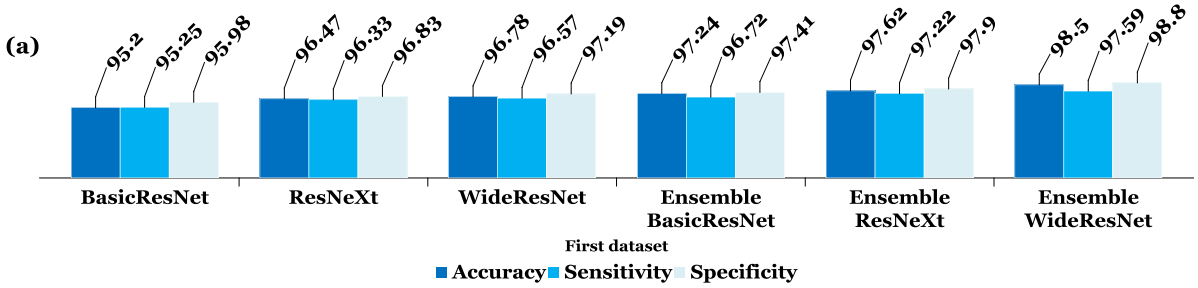

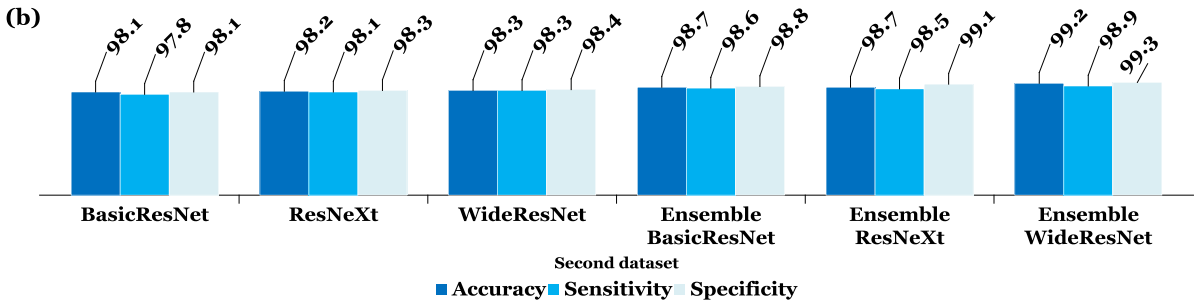

Fig. 10. As shown in section (a) and (b) for datasets 1 and 2, the accuracy, sensitivity, and specificity values are shown for an unseen sample of data.

Table 3. We evaluate our suggested model against other quantitative approaches using the same data sets.

Author(s)	Used dataset	Proposed structure	Accuracy	Computational complexity	Generalizability
Chen et al. [26]	NCT-CRC-HE-100K	MCAM	99.68%	High	Medium
		IL-MCAM	99.78%	High	Medium
Kather et al. [40]	NCT-CRC-HE-100K	VGG-16 and TL	98.70%	Low	Medium
Hamida et al. [39]	Kather texture 2016	ResNet and TL	96.60%	High	Medium
	NCT-CRC-HE-100K	ResNet and TL	99.76%	High	Medium
Ghosh et al. [38]	NCT-CRC-HE-100K	Ensemble learning based on the CNN	96.16%	High	Medium
Raju et al. [30]	Kather texture 2016	Adaptive Resnet152 model	98.38%	High	High
The proposed model	Kather texture 2016	Ensemble WideResNet	98.74%	Low	High
	NCT-CRC-HE-100K		99.23%	Low	High

Mahdi Masrori received his Bachelor and master's degrees in biomedical engineering from Hakim Sabzevari University, Sabzevar, Iran, and Azad University, Tehran, respectively, in 2020 and 2022. Currently, he is researching on experimental projects related to AJA University of Medical Sciences and cancer, Tehran, Iran.

Masoomeh Dadpay graduated with a PhD from Shahid Beheshti University, Tehran, Iran, in 1996. After graduating from Shahid Beheshti University in Tehran, Iran in 2008, she received a specialist in Pathology degree. She is currently a member of the academic faculty of the AJA University of Medical Sciences, Tehran, Iran. Additionally, she is a member of the Pathology Department at AJA University of Medical Sciences.

Khosro Rezaee received his master's and Ph.D. degrees in biomedical engineering from Hakim Sabzevari University, Sabzevar, Iran, respectively, in 2014 and 2018. At Meybod University in Meybod, Iran, he is currently an assistant professor. In his research, he focuses on image processing, pattern recognition, computer vision, medical imaging, and computer assisted diagnosis.

Hamed Naghoosi received his master's and Ph.D. microbiology degrees from Islamic Azad University, Karaj branch, Karaj, Iran. He also received his Ph.D. from Iranian Research Organization for Science and Technology (IROST), Tehran, Iran, in 2008 and 2016, respectively In Tehran, Iran, he is currently an

assistant professor at the AJA University of Medical Sciences. In his research, he focuses on different aspects of microbiology, bioinformatics, infectious diseases, and cancer research.

Hamed Bagheri received his master's degree in medical radiation engineering from Islamic Azad university, science and research branch, Tehran, Iran, in 2013. He is currently a lecturer at AJA university of medical sciences and Ph.D. candidate in medical physics at Iran university of medical sciences, Tehran, Iran. In his research, he focuses on image processing, radiotherapy, nuclear medicine and radiobiology.

Sandra Saidi is a gastroenterologist an assistant professor at AJA University of Medical Sciences, Tehran, Iran. She graduated from Tehran University of Medical Sciences in 1996. She mostly focuses on GI cancers, especially gastric cancers in her research.